The Effect of Slab Thickness on the Solidification of Low Carbon Steel in Continuous Casting Process: A Simulation Case Study

A. Pourfathi*[1]

Department of Materials Science and Engineering, Sharif University of Technology, Iran

Abstract

One of the most important and effective factors in the solidification of the steel continuous casting process is the geometry of the strand. To study the effect of this geometry, the influence of slab thickness will be investigated. To this end, a thermal model is first proposed, and its reliability is verified by simulating another paper in the literature and comparing the results with that research. In the model of the present work, thermophysical properties are calculated based on the computational thermodynamics model, CALPHAD technique. Then three different thicknesses are chosen subject to the same cooling conditions and technological parameters. Afterward, the metallurgical length and shell thickness for these thicknesses are compared. As the shell thickness is approximated by a square root function of time, holding the coefficient *K*, finally, the *K* factor of the mentioned thicknesses is extracted and compared with one another such that the higher the thickness, the higher the *K* coefficient.

Keywords : Metallurgical length, Heat transfer simulation, Continuous slab casting, Slab Thickness, Stephan problem, Coefficient *K*.

1. Introduction

In the field of materials engineering, steel continuous casting (CC) has surpassed the ingot casting process in recent decades, contributing to higher production rates, fewer casting defects, less energy waste, and higher quality of the semi-finished product. In vertical CC of steel, which is widely used around the world, the molten steel is poured from a ladle into a tundish, and then from the tundish into the primary cooling zone (water-cooled bottom-opened mold). It should be noted that the top level of melt in the mold is called the meniscus (see Fig. 1a). From the meniscus to the mold's exit, the melt solidifies partially, and a thin solid shell forms. Then the strand gradually moves down to the secondary cooling zone (SCZ) and later toward the torch cut-off point. In the SCZ, cooling water sprays sprinkle water droplets onto the surface of the strand and extract heat energy from it until the last melt droplet is solidified, or the cross-section becomes completely solid (see Fig. 1a). The distance from this point to the meniscus is called the metallurgical length (or liquid pool) [1, 2]. To be more specific, according to Fig. 1a, the yellow arc-like region inside the strand is the liquid pool, the tip of which is the last melt droplet to be solidified. The metallurgical length equals the length of the arc on which the liquid pool is outlined from the tip of the liquid pool to the meniscus. Finally, at the torch cut-off point, the strand is cut to be stored in the storehouse (for more details of the process, see Fig. 1a).

One of the most important parameters in the CC process is the quality of the final product which is affected by quite a few factors, especially the geometry of the

**Corresponding author*
Email: pourfathi.ali@gmail.com
Address:Department of Materials Science and Engineering, Sharif University of Technology, Tehran, P.O. Box 11365-9466, Iran.
1. M.Sc

strand, metallurgical parameters, and technological parameters in the continuous casting machine (CCM). To illustrate further, the geometry (especially thickness) and heat transfer parameters such as the temperature of cooling water sprays and the water flow rate in SCZ can enormously influence the existence of defects both in products and in the machine. Thanks to the increasing computing power of computers, it has become feasible to simulate and monitor heat transfer conditions in the CC process and to control both the shell thickness of the solidified shell and the defects. In the remainder of this section, several models based on this computing power will be reviewed. In the CC process, as the ladle is changed, the casting velocity must be reduced and then raised. As a result, it is highly probable that defects such as cracks and porosities, to name just two, may form. Additionally, this change affects the size of the metallurgical length and the strand temperature. Indeed, the metallurgical length, as well as the temperature field of the strand, should be fixed during any change in the CCM because an increase or decrease may culminate in the formation of breakout, porosity, cracks, and other defects. Therefore, controlling and monitoring the above-mentioned parameters has been a matter that researchers have investigated in their research studies. For this purpose, control-based models (called real-time or online models) and optimization models (also called offline models) have been proposed. In [4] and [5], the feedforward-feedback model and closed feedback loop model, respectively are proposed to minimize the temperature fluctuation due to the velocity change. In addition, works such as [6] and [7] have developed open-loop control models. During recent years, the proportional-integral-derivative (PID) control algorithm has become popular for regulating the water flow rate of sprays in SCZ and bringing down temperature disturbances, as seen in [4] and [8-13]. In [14], an alternating direction implicit algorithm (ADI), was used to maintain the surface temperature of the billet. In control methods, the high-performance computing power of computers is essential, but when computers have limited computing power and low storage memory, offline models should be used to design the CC process and its variables. Specifically, optimization models used to design the CC process are based on the inverse heat transfer problem (IHTP). Reference (or target) temperatures are measured in the CC plant, and are used as target temperatures in optimization algorithms of IHTP to determine the optimal values of heat transfer parameters in the CC process. With regards to these models, there are a great number of works in the literature; [4, 15, 16] the have applied genetic algorithms in IHTP to minimize transversal, internal, and longitudinal cracks, as well as segregation. In [17], a genetic algorithm was used to calculate the heat transfer coefficient in the mold and SCZ, but the boundary condition that describes the target temperature is a

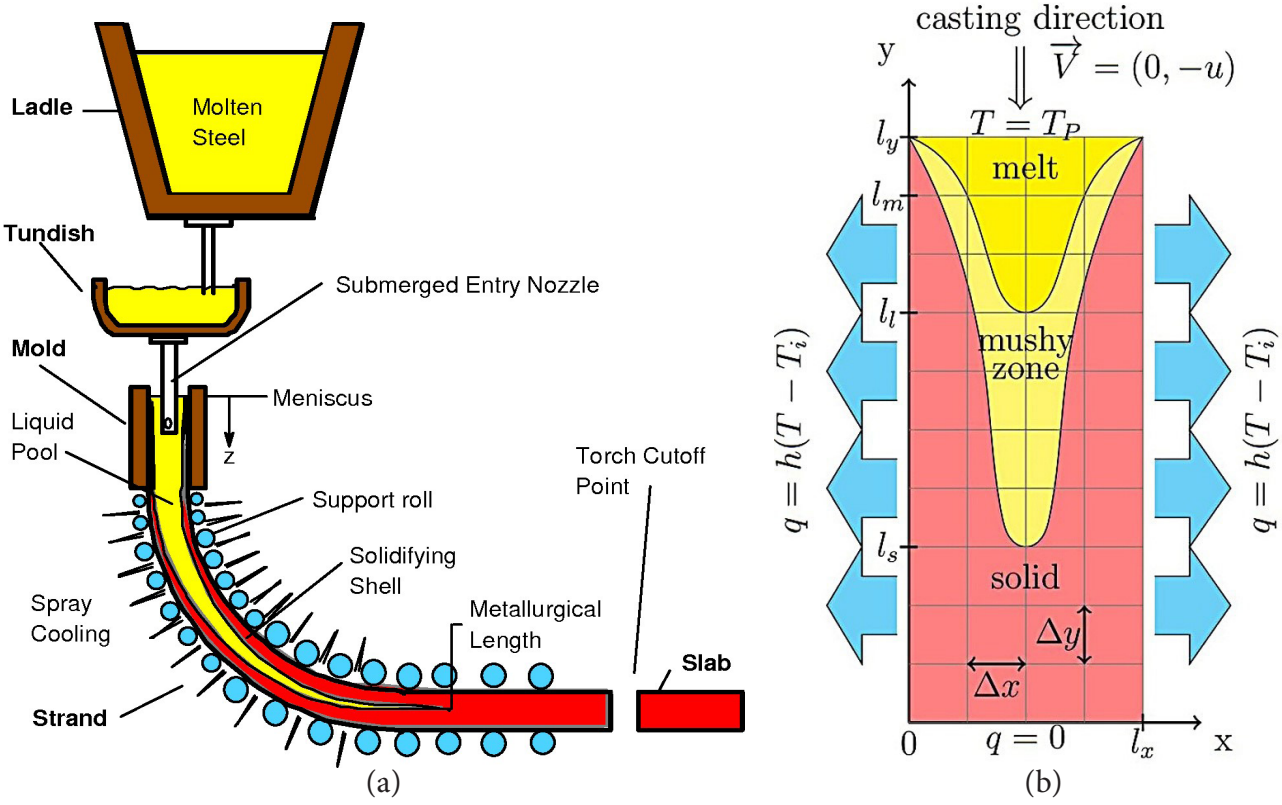

Fig. 1. (a) Schematic outline of continuous casting process [3], and (b) 2D computational domain (thickness-length cross-section from the meniscus to torch cutoff point) used in this study for the simulation of heat transfer in steel slab.

mathematical function. To maintain, the temperature field during any change in CCM, by setting corner and/or central temperatures as target points, other algorithms have been used such as: Nelder-Mead algorithm [18], multi-objective optimization algorithm [19], particle swarm optimization (PSO) algorithm [20], predictive GPU-based weighted least square model [21], neural network (NN) which showed that the PID method is less efficient [22], artificial intelligence heuristic search models [23, 24], modified proximal bundle algorithm [25], Broyden–Fletcher–Goldfarb–Shanno (BFGS) algorithm [26], Levenberg−Marquardt [21, 27, 28], and sequential quadratic programming (SQP) [29]. In [30], the influence of changing casting velocity on thermomechanical behavior while maintaining metallurgical length was studied. To be more precise, the method used in [30] is based on fixing transported heat energy to maintain a constant metallurgical length for different casting velocities with heat transfer coefficients calculated according to an empirical relation. As previously mentioned, geometry is an important factor that influences the temperature field, metallurgical length, and the quality of the strand, but there have been no studies on the effect of strand thickness in the literature.

In the present work, we study the effect of different strand thicknesses on the metallurgical length, temperature field, and solidification of a low-carbon steel grade. To elaborate, section 2, expresses the mathematical model used in this study will be expressed. In section 3, the mathematical model is implemented and validated using a reference including the simulation of the low-carbon steel. The thermophysical properties are obtained from a thermodynamic computation method called CALPHAD[2]. Next, three different thicknesses are assumed, and the simulation is run for these thicknesses. In section 4, the results will be discussed, showing that the metallurgical length computed using the proposed simulation model conforms well with an analytical square root formula with a coefficient. Furthermore, as this formula is commonly used in continuous casting plants to predict metallurgical length easily, the coefficient will be calculated for each test case, and their correlation with slab thickness will be discussed and investigated.

2. Mathematical Description

As is common in the literature, the heat transfer equation is applied for thermal simulation. The heat transfer equation is used in the present work to simulate solidification and the distribution of temperature in a slab. Beforehand, several assumptions are considered in this study as follows:

1) The process is assumed to be a in quasi-steady state; thus, the quasi-steady state heat transfer equation will be solved because it is computationally less costly.

2) The slab is assumed to be vertical without any curve or bending; therefore, plastic strain or elastic strain is not considered in the model.

3) There is no roller in contact with the strand.

4) The length of the slab (along the casting direction) is higher than its thickness and width. The width of the strand is larger than the thickness, and as a result, the thermal gradient along the width direction is ignored in the heat transfer equation (simulation will be conducted just for the length-thickness cross-section).

5) The effect of fluid flow is ignored.

6) The casting velocity is assumed to be constant (but slab thickness is changed, and its effect will be studied in this study).

7) The density, thermal conductivity, and specific heat capacity for both liquid and solid phases are not assumed to be identical or constant. Instead, the thermophysical properties are extracted directly as a function of temperature based on a computational thermodynamics method called CALPHAD approach, which stems from global minimization of Gibbs energy. More details are described in section 3.

The correspondent computational domain of the strand is denoted as Ω, and its boundary, $\partial\Omega$, is divided into four partitions: lateral boundary (or cooling region), Γ_l, top boundary (or meniscus), Γ_t, bottom boundary (or torch cut-off point), Γ_b, (in other words, $\partial\Omega=\Gamma_l\cup\Gamma_t\cup\Gamma_b$), see Fig. 1b Following [4, 29, 31-35], the quasi-steady state heat transfer equation based on the enthalpy method is as follows:

$$\rho c_{pe}\vec{V}.\nabla T = \nabla.(k\nabla T) \quad \text{in} \quad \Omega \qquad \text{Eq. (1)}$$

$$T = T_p \quad \text{on} \quad \Gamma_t \qquad \text{Eq. (2)}$$

$$-k\ \nabla T.\vec{n} = 0 \quad \text{on} \quad \Gamma_b \qquad \text{Eq. (3)}$$

$$-k\ \nabla T.\vec{n} = h\ (T - T_i) \quad \text{on} \quad \Gamma_l \qquad \text{Eq. (4)}$$

Where $\vec{V}$, T, k, c_{pe}, ρ, T_i, h, $\vec{n}$ and T_p denote casting velocity, temperature, thermal conductivity, effective specific heat capacity, density, cooling water temperature, heat transfer coefficient, outward unit normal, and pouring temperature, respectively (both T_i and h vary spatially). The casting velocity, $\vec{V} = (0, -u)$, is such that the value of $u > 0$, and the strand is cast along the $-\vec{y}$ direction (see Fig. 1b). In many works, the effective specific heat capacity, c_{pe}, (using the enthalpy method) is obtained as follows:

$$c_{pe} = c_p + L_f \frac{df_l(T)}{dT} \qquad \text{Eq. (5)}$$

Where $f_l(T)$, c_p, and L_f denote the liquid volume fraction, heat capacity, and latent heat of fusion, respectively. Although liquid volume fraction, f_l(T), and latent heat of fusion, L_f, as well as other thermophysical properties, are simply interpolated and assumed constant in some re-

2 CALculation of PHAse Diagrams

search studies in the literature (for example [31]), these thermophysical properties should not be simplified as constant or as an explicit function of temperature because in practice, phenomena such as solid-state phase transformation, the peritectic reaction in peritectic grades, and so on, occur. Because of these restrictions, to consider the effects of these phenomena, the thermophysical properties are calculated based on the CALPHAD technique which is explained in more detail in the next section [36].

3. Numerical Implementation

In this section, the presented model is implemented using a reference in the literature, and our simulation is conducted for a thickness of 23cm, and the results of our simulation are compared with those of the reference to validate the simulation model. Then, the proposed model is applied for thicknesses of 18cm and 28cm. Henceforth, the simulations supposed to be implemented for thicknesses 23cm, 18cm, and 28cm are symbolized as test case #1, test case #2, and test case #3, respectively.

To find the temperature distribution of test case #1, a heat transfer simulation based on the mathematical model described previously will be conducted. First, the thermodynamic properties are extracted from the CALPHAD model using the JMatPro package, see Fig. 2. The CALPHAD approach is an interesting thermodynamic technique in the field of materials science and engineering that can predict thermophysical properties as a function of temperature. In fact, given an alloy with a definite chemical analysis, it is possible to globally minimize the free energy by employing a database including free energies of each phase. As a result, this method paves the way to calculate thermodynamics equilibria such as phase diagrams and thermophysical properties for commercial steel grades as well as for multi-component alloys [36]. Then the geometry, pouring temperature, solidus temperature, liquidus temperature, water flow rates of nozzles in SCZ, and cooling water temperature of the nozzles are extracted from reference [37], see Table 1 and Table 2. l_z, l_x, l_y, l_m, n_x, n_y, u, T_l, and T_s, respectively denote the width of the slab, the thickness, machine length (the length of the slab, precisely from the meniscus to the torch cutoff), the mold length, mesh size on the $\vec{x}$ axis, the mesh size on the $\vec{y}$ axis, the value of casting velocity, liquidus temperature, and solidus temperature. Also, the chemical composition of the low-carbon steel grade used in this study is listed in Table 3. The thickness of test case #1 (which is simulated in this subsection), as well as test cases #2 and #3 (which will be studied in the next subsection) are listed in Table 4. As far as heat transfer on the interphase between the mold and the strand is concerned, according to reference [37], the following heat flux is used

$$q = 2400000 - 346000\sqrt{1_m/u} \qquad \text{Eq. (6)}$$

Where q denotes heat flux.

It should be noted that in [37] only the water volume in SCZ is given. However, in this study using Nozaki's relation [38], the heat transfer coefficients are computed in each segment of SCZ as Eq. (7):

$$h = \frac{1570\ w^{0.55}(1-0.0075\ T_i)}{\beta} \qquad \text{Eq. (7)}$$

Where w and β denote the water flow rate and the machine-dependent calibration factor. The water volume and machine-dependent calibration factor are extracted from [37], listed in Table 5. By the given water volume, water flow rate, w, can be obtained; then, using the relation (7), the heat transfer coefficient in each segment of SCZ is calculated. The computed heat transfer coefficient for all spray segments is symbolized as $h_{working}$ hereafter. The heat transfer coefficient and cooling water temperature (of cooling nozzles in SCZ) are the same (as T_i) for all three cases.

Table 1. Geometry, mesh size parameters, casting velocity, and cooling water temperature of nozzles used in this study and [37].

l_z (m)	l_x (cm)	l_y (m)	l_m (m)	n_x	n_y	u (m/min)	T_i (ºC)
1.25	23	30	0.9	40	100	1.1	25

Table 2. Pouring Temperature, solidus Temperature, and liquidus Temperature of the steel grade used in this study [37].

T_l (ºC)	T_s (ºC)	T_P (ºC)
1519	1453	1577

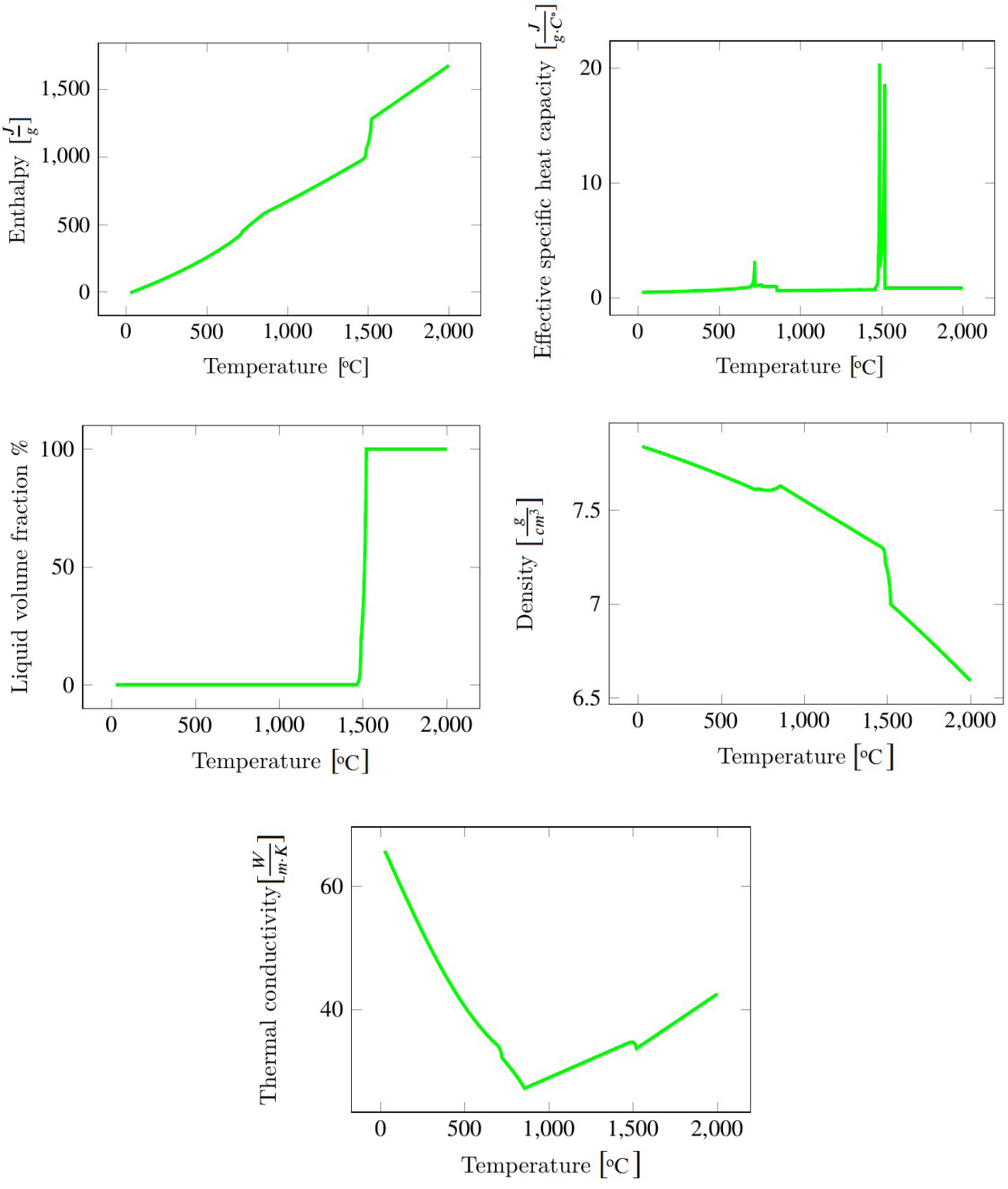

Fig. 2. Thermophysical properties of the steel grade used in this study. All properties are based on the CALPHAD method and extracted from the JMatPro package.

Table 3. Chemical analysis (in percent) of the low carbon steel grade studied both in [37] and in the present work.

Fe	C	Si	Mn	S	P	Al	N
Base	0.15	0.15	0.25	0.015	0.02	0.002	0.016

Table 4. The thicknesses of three test cases studied in the present work.

Test case NO.	Thickness (cm)
#1	23
#2	18
#3	28

Table 5. The length, water volume, and calibration factor of each spray cooling segment along SCZ [37].

Sprays	Length (m)	Water volume (L/min)	Calibration factor
segment 1	2.96	367.8	4
segment 2	1.819	343.7	4.23
segment 3	1.819	293.9	4.78
segment 4	3.789	195.2	2.78
segment 5	6.094	260.3	2.89
segment 6	6.945	225.5	2.62
segment 7	4.62	140.6	3.06
segment 8	2.31	60	2.89

3.1 Model Validation

By conducting the heat transfer simulation using the data from the previous section for test case #1, the results will be explained in the following. In Fig. 3, the comparison of surface temperature and centerline temperature between research [37] and the simulation of the model in test case #1 in this study shows a reasonable and acceptable agreement between the simulation of the thermal model in this study and research [37]. According to Fig. 4 and the red graph as well as the blue graph in Fig. 3, in our simulation, the calculated metallurgical length of test case #1 equals 20.0317653m, which is close to that obtained in [37] as 19.9m. In Fig. 4, the black profile is the result of the simulation in the present work, and green and orange points are data presented in [37]. Fig. 4 shows that the shell thickness at three different distances from the meniscus is approximately close to the simulated profile in the present work. The difference in shell thickness between our simulation and experimental results is 6%. In addition, there is a little but acceptable difference between the surface temperature distribution simulated in this study and that of [34] in the worst case of 7% (see black and green graphs of Fig. 3). This difference is due to the fact that CALPHAD thermodynamic calculations mentioned in the previous section are used in this study, but constant values for thermophysical properties are applied in research [37].

Furthermore, Fig. 4 shows a close approximation of the calculation of shell thickness among test case #1 in this study, simulation in [37], and measurement using an experiment in [37]. The results of test case #1, shown in Fig. 3 and Fig. 4 confirm the acceptable accuracy of the presented simulation model in this study. Next, using the applied data in the simulation of test case #1, simulation is implemented for both cases by reducing and raising the slab thickness to 18cm (test case #2) and 28cm (test case #3), respectively and the results will be studied in the next section.

4. Results and Discussion

This section aims to evaluate the performance and functionality of the presented model. As per the previous sections, the thicknesses of 18cm and 28cm correspond to test case #2 and test case #3, respectively. Additionally, the interfacial boundary between the slab and both the mold and SCZ is divided into two partitions; in other words, $\Gamma_l = \Gamma_{lm} \cup \Gamma_{ls}$ where Γ_{lm} is the contact region between the slab and mold, and Γ_{ls} is the contact region between the slab and SCZ. The heat transfer in these regions is the same as that in test case #1. In the following, shell thickness (or solid) profiles, metallurgical length, temperature distribution, and liquid volume fraction distribution will be discussed. Moreover, the constant coefficient K in the square root function mentioned at the end of section 1 will be determined.

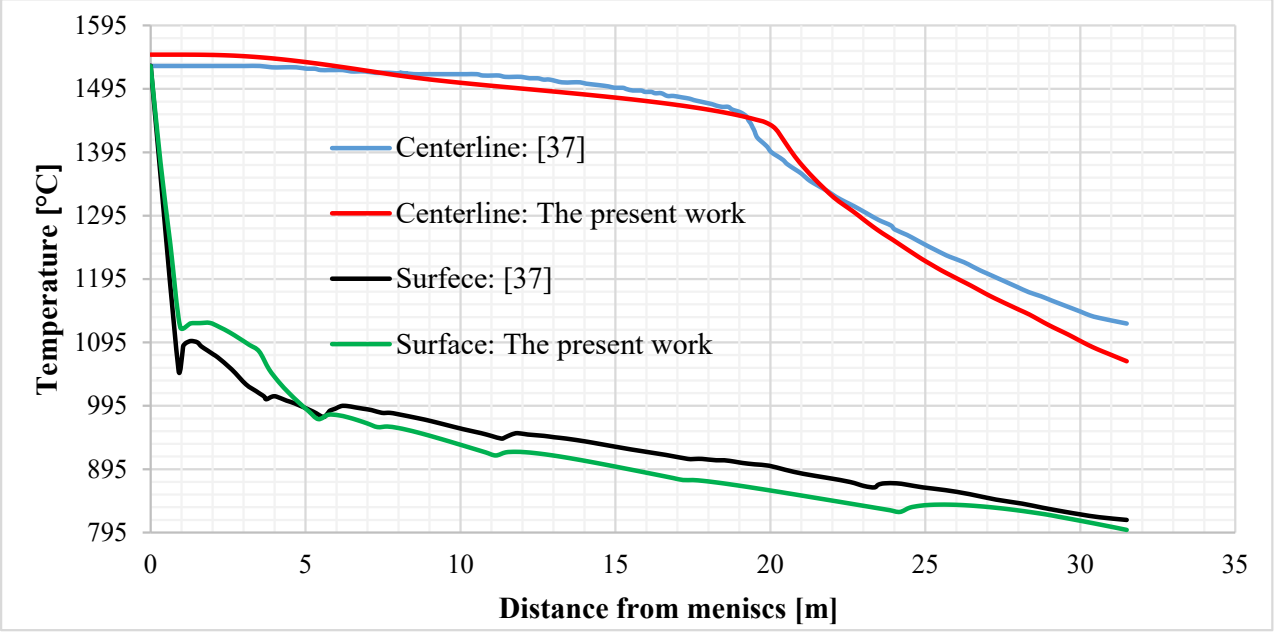

Fig. 3. Comparison of simulated centerline temperature profiles (red and blue) and simulated surface temperature profiles (black and green) between the present work and [37] for test case #1 with respect to distance from the meniscus.

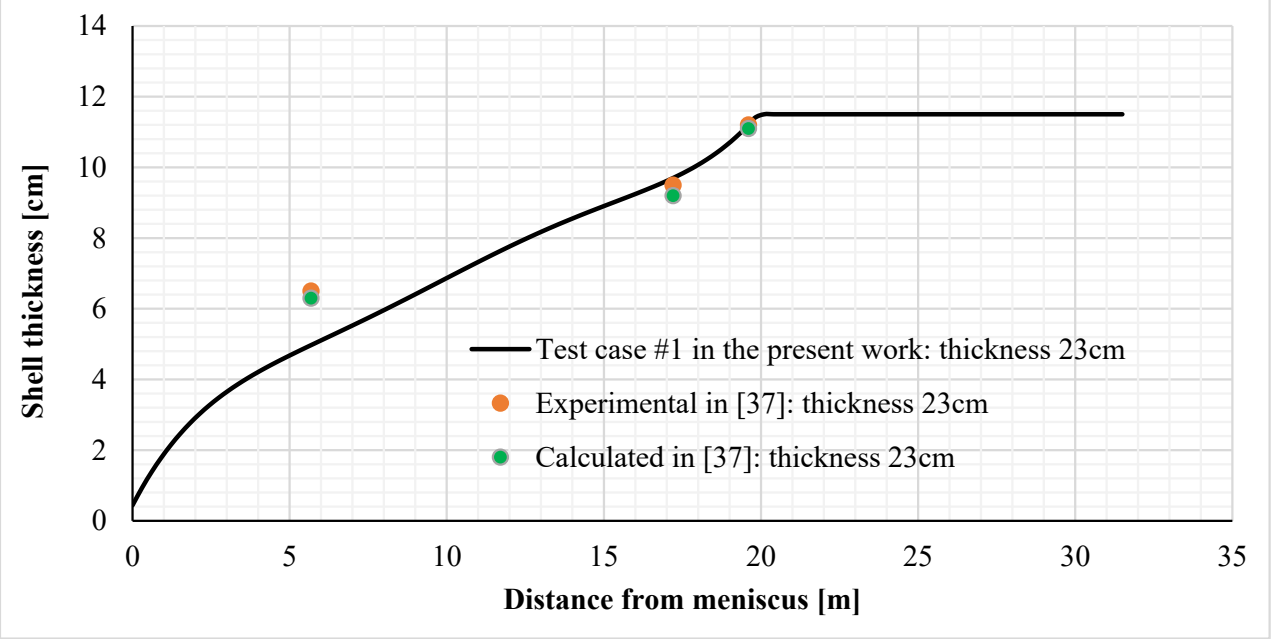

Fig. 4. Comparison of Shell thickness with respect to distance from the meniscus. The black curve corresponds to test case #1 simulation in this study; both the experimental data (orange points) and simulated data (green points) are extracted from [37].

4.1 Shell thickness

In Fig. 5, the variation of shell thickness as a function of distance from the meniscus for all test cases #1, #2, and #3 is shown. According to the plot, raising the thickness of the slab from 18cm to 28cm, increase the shell thickness profile correspondingly, especially from segment 3 to the torch cut-off point; however, their difference is minimal near the meniscus and segments 1 and 2.

4.2 Metallurgical Length

Using $h_{working}$, the metallurgical length for test cases #2 and #3 is approximately 12.5m and 28.78m, see Figs. 6c and 6a, respectively. With regards to test cases #2 and #3, in which the thickness is reduced and raised respectively, the metallurgical length approaches 12.5m and 28.78m in order. Additionally, Fig. 6 shows the contour plots of the temperature field corresponding to the liquid volume fraction shown in Fig. 6. Accordingly, it is evident that the metallurgical length depends on the slab thickness such that by raising the slab thickness, the metallurgical length also increases.

4.3 Analysis of Square Root Function

In the literature, it is widely agreed that the solid profile of the strand approximately conforms to a square root function. In fact, it is assumed that the solidification front is moving interphase between liquid and solid phases. Considering the solidification front as a moving boundary, a two-dimensional Stephan problem has been solved in the literature [6,39-41], contributing to an analytical formula for the calculation of metallurgical length as follows:

$$x_s = K\sqrt{t} \quad \text{or} \quad x_s = K\sqrt{\frac{D}{u}} \qquad \text{Eq. (8)}$$

Where x_s, D, and t denote the shell thickness, the distance from the meniscus, and time, respectively. This criterion expresses the approximate position of the solid shell; more importantly, the formula can determine the size of the metallurgical length. It is worth noting that this formula is widely used to compute metallurgical length and the location of segregation (after the traditional Baumann sulfur printing test) in the industry. The most significant challenge for casting plants is determining the K factor in their casting case because K depends on machine variables, chemical composition, and the geometry of the strand, among others.

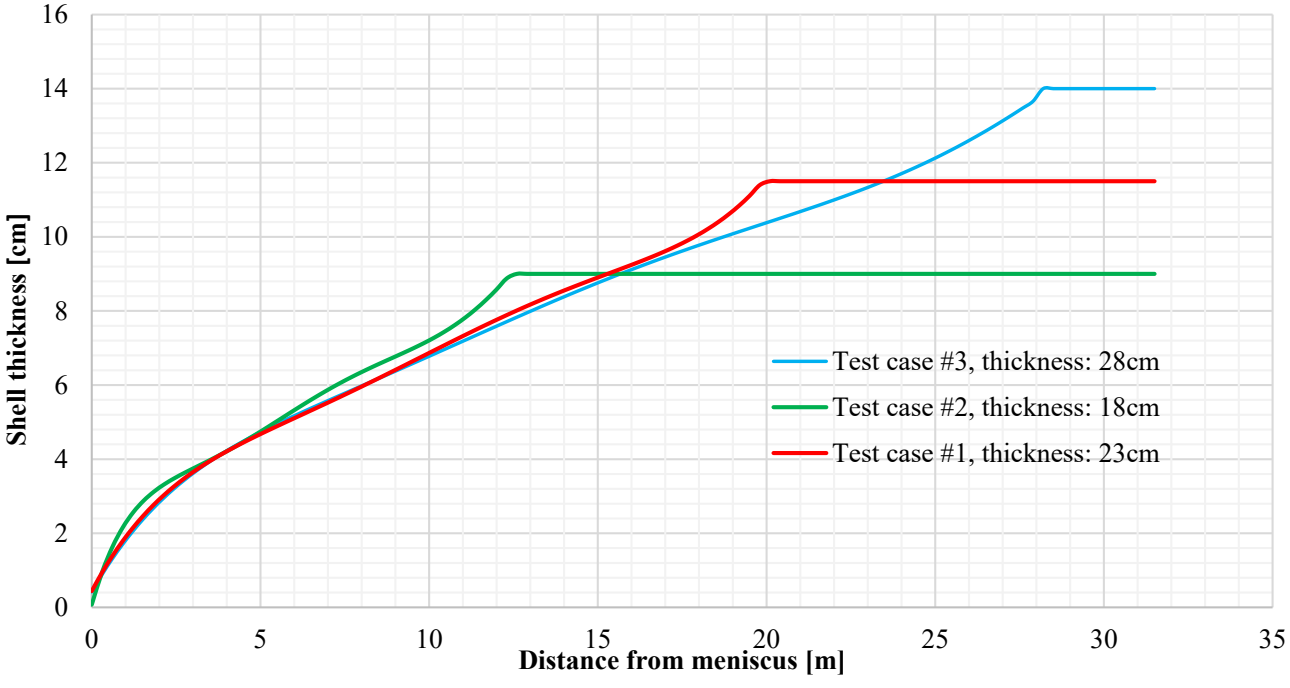

Fig. 5. Simulated shell thickness with respect to distance from meniscus for test case #2 (18cm; green), for test case #1 (23cm; red), and for test case #3 (28cm; blue) in this study.

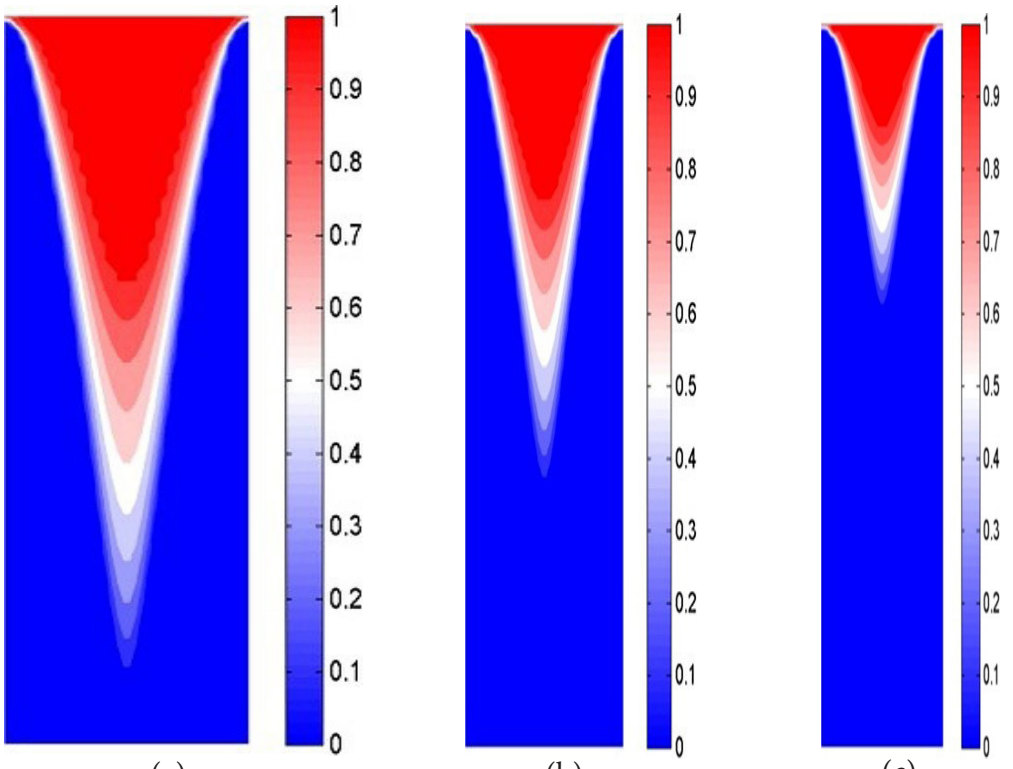

Fig. 6. Contour plots of liquid volume fraction at the end of simulation: a) test case #3 b) test case #1, and c) test case #2 in this study.

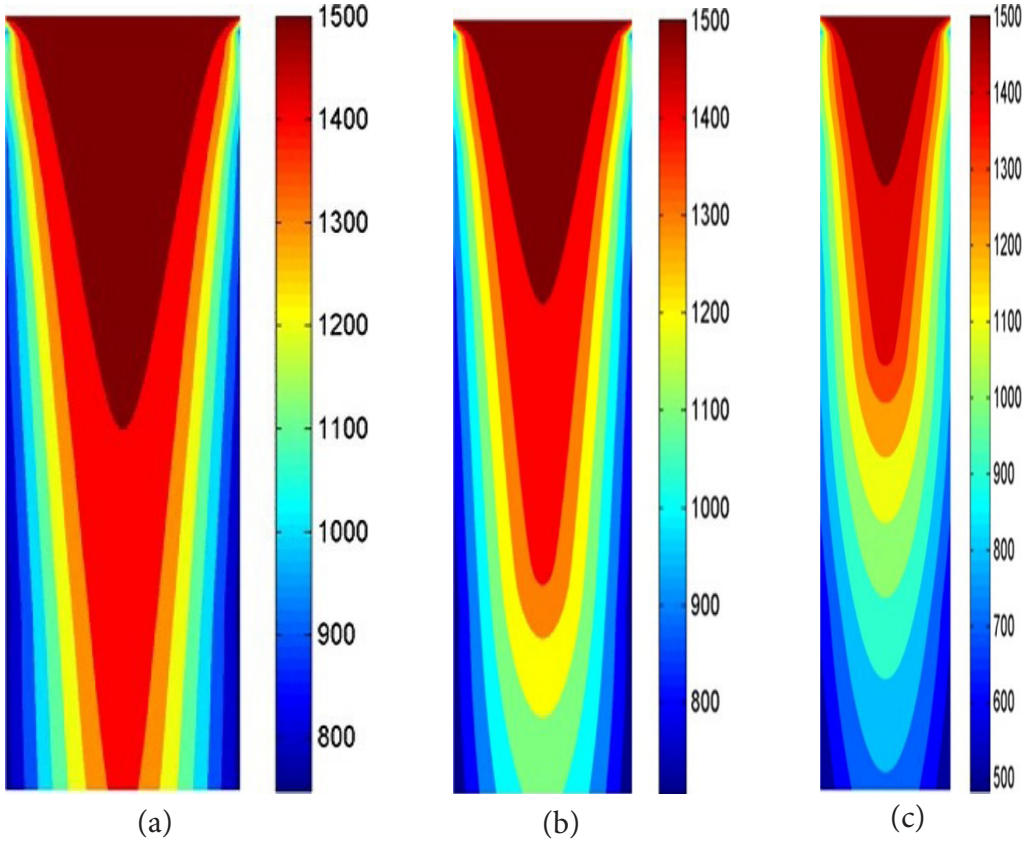

Fig. 7. Contour plots of temperature distribution at the end of simulation: a) test case #3 b) test case #1, and c) test case #2 in this study.

In this section, coefficient K is extracted using the mathematical curve fitting technique for test cases #1, #2, and #3, and the correlation between slab thickness and the coefficient K will be studied. In fact, K is determined such that criterion (8) predicts the metallurgical length for continuous casting. To this end, the coefficient K will be calculated using the metallurgical length obtained from shell thickness profiles. Regarding test case #1 (23cm), Fig. 8 shows the shell thickness with respect to the distance from the meniscus for both the simulated (black curve) and the x_s function (red curve). Using the simulated solid profile, the coefficient K is determined to be K_{23}=26.8370 m. min$^{-0.5}$ in order to predict the metallurgical length for test case #1. The relative absolute error equals 11 % which is acceptable because the size of the metallurgical length, not the exact solid profile in different positions, is important. Fig. 9, shows the shell thickness with respect to distance from the meniscus for test case #2 (18cm); similar to test case #1, using the simulated solid profile (black curve) and x_s function (red), the coefficient K is calculated K_{18}= 26.5226 m. min$^{-0.5}$. The relative absolute error equals 13% in test case #2.

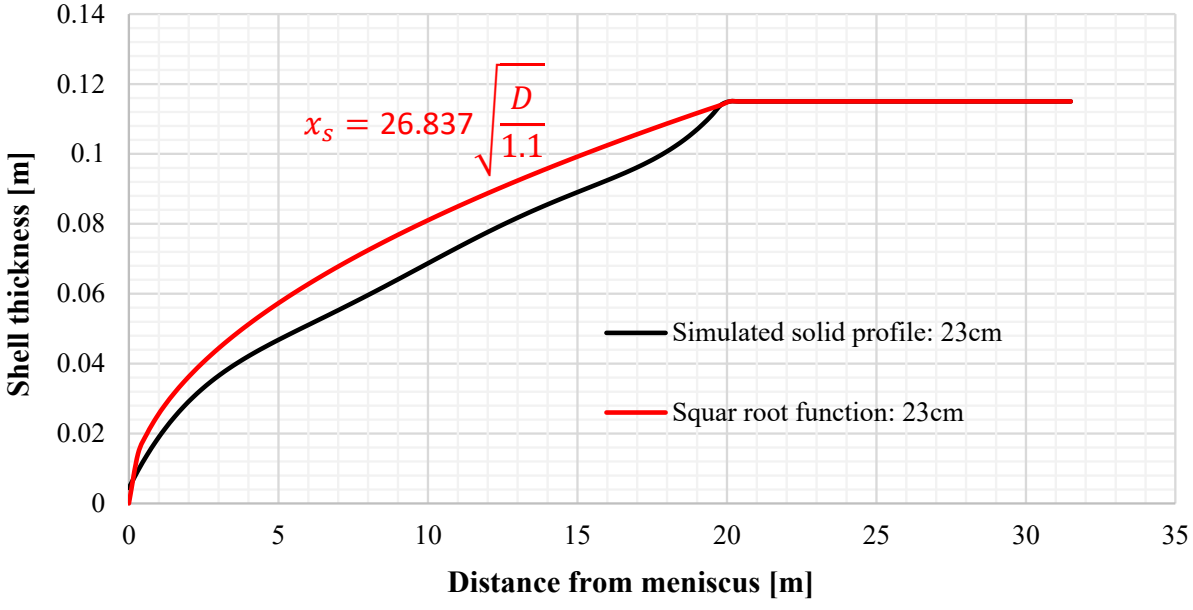

Fig. 8. Simulated shell thickness with respect to distance from meniscus (black) and fitted square root function (red) for test case #1 (23cm) in this study.

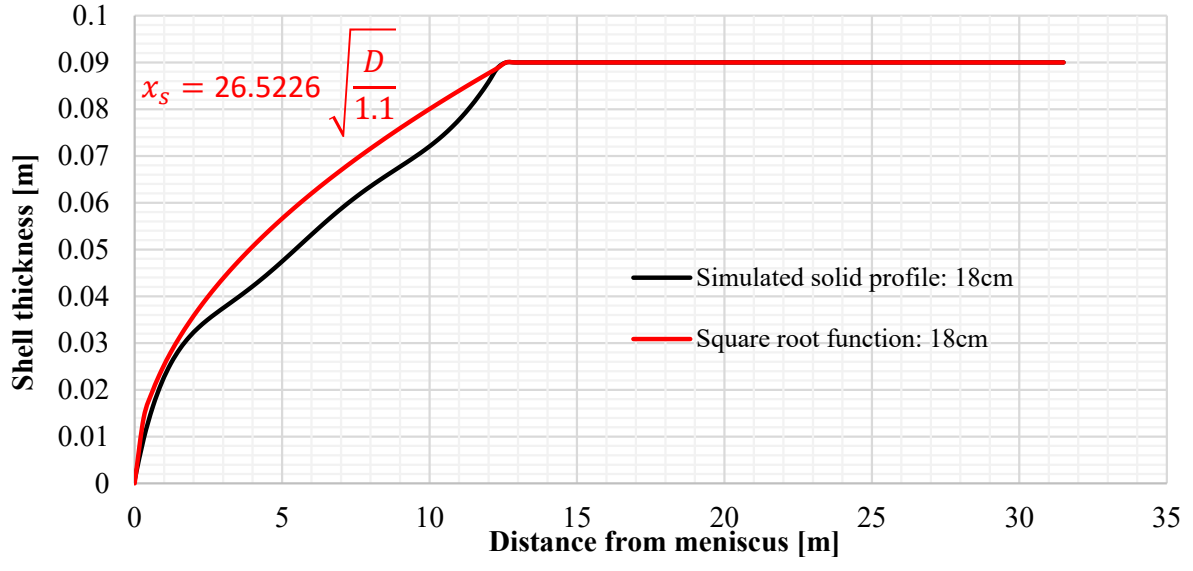

Fig. 9. Simulated shell thickness with respect to distance from meniscus (black) and fitted square root function (red) for test case #2 (18cm) in this study.

Finally, Fig. 10 shows the simulated shell thickness as a function of the distance from the meniscus and the x_s function. Similar to the previous test cases, the coefficient K is computed as K_{28}= 27.6252 m. min$^{-0.5}$ and the relative absolute error is approximately 11%.

By comparing the thicknesses and their corresponding calculated factors in Table 6, it is obvious that by increasing the slab thickness, the coefficient K in Eq. (8), which determines the metallurgical length, rises proportionally.

5. Conclusions

Steel continuous casting process is sensitive to the change in slab thickness, which can lead to the justification of cooling parameters. It is crucial for steel continuous casting plants to predict the shell thickness, metallurgical length, and the K factor in the square root function, used to predict metallurgical length in steel continuous slab casting as slab thickness varies. In this study, a two-dimensional heat transfer model coupled with the CALPHAD model to determine thermophysical properties we used to investigate the effect of three slab thicknesses on the metallurgical length and shell thickness. Then the values of the K factor for each thickness were extracted using curve fitting technique. Accordingly, the higher the slab thickness, the longer the metallurgical length. In order words, the coefficient K in the square root function increases as far as the slab thickness grows.

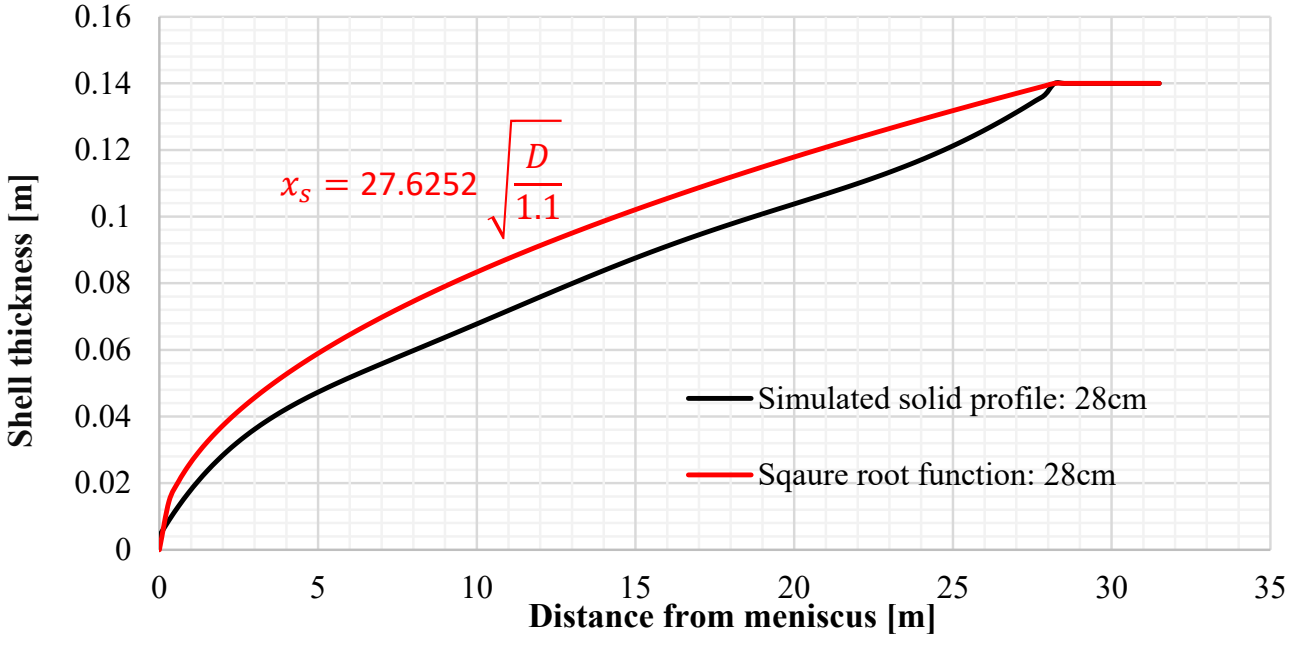

Fig. 10. Simulated shell thickness with respect to distance from meniscus (black) and fitted square root function (red) for test case #3 (28cm) in this study.

Table 6. The calculated coefficient K, metallurgical length, and thickness for test cases in this study.

Test case NO.	Thickness (cm)	Coefficient K (m. min$^{-0.5}$)	Metallurgical length (m)
#2	18	26.5226	12.50
#1	23	26.8370	20.03
#3	28	27.6252	28.78

Acknowledgments

The author would like to thank Professor Ruohollah Tavakoli for suggesting the writing of the present work.

Nomenclature

c_{pe}	Specific heat capacity
D	Distance from meniscus
f_l	Liquid volume fraction
h	Heat transfer coefficient
K	The coefficient in the square root function of time and shell thickness
k	Thermal conductivity
L_f	Latent heat of fusion
l_m	The thickness of the mold
l_x	The thickness of the slab
l_y	The length of the slab
$\vec{n}$	The outward unit normal vector on a surface
n_x	Mesh size index along the thickness
n_y	Mesh size along the length
q	Heat flux
T	Temperature
T_i	Cooling water temperature
T_P	Pouring temperature
t	Time
u	The absolute value of casting speed
$\vec{V}$	Casting velocity vector
w	Water flow rate
x_s	Shell thickness
β	Calibration factor of continuous casting machine
Γ_b	The bottom boundary of the computational domain
Γ_l	The lateral boundary of the computational domain
Γ_t	The top boundary of the computational domain
Δx	The size of the computational cell along the thickness direction
Δy	The size of the computational cell along the length direction
ρ	Density
Ω	The computational domain corresponding to the slab

Reference

[1] J. Hejazi, Ingot Casting, Irainan Foundarymen Society, 1982, (in Persian).
[2] B. Petrus, D. Hammon, M. Miller, B. Williams, A. Zewe, Z. Chen, J. Bentsman, B. Thomas, Newmethod to measure metallurgical length and application to improve computational models, Iron and Steel Technology Conference and 7th International Conference on the Science and Technology of Ironmaking, Cleavlad , USA, 2015.
[3] X. Huang, B. Thomas, Modeling of steel grade transition in continuous slab casting processes, Metallurgical Transactions B. 24 (1993) 393-379. https://doi.org/10.1007/BF02659140.
[4] C. Santos, J. Spim, A. Garcia, Mathematical modeling and optimization strategies (genetic algorithm and knowledge base) applied to the continuous casting of steel, Engineering Applications of Artificial Intelligence. 16 (2003) 511-527. https://doi.org/10.1016/S0952-1976(03)00072-1.
[5] M. Long, D. Chen, J. Zhang, Q. Ouyang, Novel online temperature control system with closed feedback loop for steel continuous casting, Ironmaking & Steelmaking. 38 (2011) 620-629. https://doi.org/10.1179/1743281211Y.0000000042.
[6] L. Klimeš, J. Štětina, A rapid GPU-based heat transfer and solidification model for dynamic computer simulations of continuous steel casting, Journal of Materials Processing Technology. 226 (2015) 1-14. https://doi.org/10.1016/j.jmatprotec.2015.06.016.
[7] S. Louhenkilpi, M. Mäkinen, S. Vapalahti, T. Räisänen, J. Laine, 3D steady state and transient simulation tools for heat transfer and solidification in continuous casting, Materials Science and Engineering: A. 413(2005) 135-138. https://doi.org/10.1016/j.msea.2005.08.153.
[8] K. Zheng, B. Petrus, B. G. Thomas, J. Bentsman, Design and implementation of a real-time spray cooling control system for continuous casting of thin steel slabs, Proceeding AISTech Steelmaking Conference, Indianapolis, 2007.
[9] J. Yang, Z. Xie, Z. Ji, H. Meng, Real-time heat transfer model based on variable non-uniform grid for dynamic control of continuous casting billets, ISIJ international. 54 (2014) 328-335. https://doi.org/10.2355/isijinternational.54.328.
[10] B. Petrus, K. Zheng, X. Zhou, B. Thomas, J. Bentsman, Real-time, model-based spray-cooling control system for steel continuous casting, Metallurgical and materials transactions B. 42 (2011) 87-103. https://doi.org/10.1007/s11663-010-9452-7.
[11] T. Männikkö, E. Laitinen, P. Neittaanmäki, Real-time simulation and control system for the continuous casting process, in: H.-H. Sebastian, K.Tammer (eds), System Modelling and Optimization, Springer-verlag Berlin Heidelberg GmbH, 1990, pp.809-817.
[12] E. Laitinen, P. Neittaanmäki, T. Männikkö, On the Real-time Simulation and Control of the Continuous Casting Process, In: J. Manley, S. McKee, D. Owens (eds), Proceedings of the Third European Conference on Mathematics in Industry, Springer-verlag Berlin Heidelberg GmbH, 1990, pp.401–408.
[13] L. Guo, Y. Tian, M. Yao, H. Shen, Temperature distribution and dynamic control of secondary cooling in slab continuous casting, International Journal of Minerals, Metallurgy and Materials. 16 (2009) 626-631. https://doi.org/10.1016/S1674-4799(10)60003-9.
[14] M. Jauhola, E. Kivela, J. Konttinen, E. Laitinen, S. Louhenkilpi, Dynamic secondary cooling model for a continuous casting machine, Proceeding 6th International Rolling Conference, Dusseldorf, Germany, 1994.
[15] Y. Zhai, Y. Li, B. Ma, C. Yan, Z. Jiang, The optimisation of the secondary cooling water distribution with improved genetic algorithm in continuous casting of steels. 19 (2015) 26-31. https://doi.org/10.1179/1432891715Z.0000000001362.
[16] K. Worapradya, P. Thanakijkasem. Optimum spray cooling in continuous slab casting process under productivity improvement, IEEE International Conference on Industrial Engineering and Engineering Management, Hong Kong, 2009.
[17] D. Słota, Identification of the cooling condition in 2-D and 3-D continuous casting processes, Numerical Heat Transfer Part B: Fundamentals. 2 (2009) 155-176. https://doi.org/10.1080/10407790802605232.
[18] B. Filipic, E. Laitinen, Model-based tuning of process parameters for steady-state steel casting, Informatica an international journal of computing and informatics. 29 (2005) 2005 491-496.
[19] K. Cho, B. Kim, Numerical analysis of secondary cooling in continuous slab casting, Journal of Materials Science and Technology. 24(2008) 389-390. https://doi.org/10.1016/S0924-0136(01)00654-9.
[20] F. Camisani-Calzolari, I. Craig, P. Pistorius, Specification framework for control of the secondary cooling zone in continuous casting, ISIJ international. 38 (1999) 7131-7136. https://doi.org/10.2355/isijinternational.38.447.
[21] J. Zhang, D. Chen, C. Zhang, S. Wang, W. Hwang, Dynamic spray cooling control model based on the tracking of velocity and superheat for the continuous casting steel, Journal of Materials Processing Technology. 229 (2016) 651-658. https://doi.org/10.1016/j.jmatprotec.2015.10.015.
[22] N. Cheung, A. Garcia, The use of a heuristic search technique for the optimization of quality of steel billets produced by continuous casting, Engineering Applications of Artificial Intelligence. 14 (2001) 229-238. https://doi.org/10.1016/S0952-1976(00)00075-0.
[23] D. Van der Spuy, I. Craig, P. Pistorius, An optimization procedure for the secondary cooling zone of a continuous billet caster, Journal of the Southern African Institute of Mining and Metallurgy. 99 (1999) 49-54. https://hdl.handle.net/10520/AJA0038223X_2613.

[24] T. Mauder, C. Sandera, J. Stetina, Optimal control algorithm for continuous casting process by using fuzzy logic, Steel Research International. 86 (2015) 785-798. https://doi.org/10.1002/srin.201400213.
[25] Y. Wang, X. Luo, Y. Yu, Q. Yin, Evaluation of heat transfer coefficients in continuous casting under large disturbance by weighted least squares Levenberg-Marquardt method, Applied Thermal Engineering. 111 (2017) 989-996. https://doi.org/10.1016/j.applthermaleng.2016.09.154.
[26] Y. Yu, X. Luo, Estimation of heat transfer coefficients and heat flux on the billet surface by an integrated approach, International Journal of Heat and Mass Transfer. 90 (2015) 645-653. https://doi.org/10.1016/j.ijheatmasstransfer.2015.07.008.
[27] T. Männikkö and M. Mäkelä, Nonsmooth penalty techniques in control of the continuous casting process, in: P. Neittaanmaki (eds), Numerical Methods for Free Boundary Problems, Springer-Basel AG, 1991, pp.297-307. https://doi.org/10.1007/978-3-0348-5715-426.
[28] B. Lally, L. Biegler, H. Henein, Optimization and continuous casting: Part II Application to industrial casters, Metallurgical Transactions B. 22 (1991) 649-659. https://doi.org/10.1007/BF02679020.
[29] S. Louhenkilpi, E. Laitinen, R. Nieminen, Real-time simulation of heat transfer in continuous casting, Metallurgical Transactions B. 24 (1993) 685-693. https://doi.org/10.1007/BF02673184.
[30] M. Bellet, L. Salazar-Bbetancourt, O. Jaouen, F. Costes, Modelling of water spray cooling Impact on thermomechanics of solid shell and automatic monitoring to keep metallurgical length constant, European continuous casting conference (8th ECCC), Austrian society for metallurgy and materials, 2014.
[31] R. Tavakoli, Smooth modeling of solidification based on the latent heat evolution approach, The International Journal of Advanced Manufacturing Technology, 88 (2017) 3041-3052. https://doi.org/10.1007/s00170-016-9012-7.
[32] M. Sadat, A. H. Gheysari, S. Sadat, The effects of casting speed on steel continuous casting process, Heat and mass transfer. 47 (2011) 1601-1609. https://doi.org/10.1007/s00231-011-0822-8.
[33] E. Majchrzak, Numerical simulation of continuous casting solidification by boundary element method, Engineering Analysis with Boundary Elements. 11 (1993) 95-99. https://doi.org/10.1016/0955-7997(93)90028-J.
[34] Z. Han, D. Chen, K. Feng, M. Long, Development and application of dynamic soft-reduction control model to slab continuous casting process, ISIJ international. 50 (2010) 1637-1643. https://doi.org/10.2355/isijinternational.50.1637.
[35] M. Alizadeh, A. J. Jahromi, O. Abouali, A new semi-analytical model for prediction of the strand surface temperature in the continuous casting of steel in the mold region, ISIJ international. 48 (2008) 161-169. https://doi.org/10.2355/isijinternational.48.161.
[36] A. Pourfathi, R. Tavakoli, Thermal optimization of secondary cooling systems in the continuous steel casting process, International Journal of Thermal Sciences. 183 (2023) 107860. https://doi.org/10.1016/j.ijthermalsci.2022.107860.
[37] Y. Yu, X. Luo, H. Y. Zhang, Q. Zhang, Dynamic optimization method of secondary cooling water quantity in continuous casting based on three-dimensional transient nonlinear convective heat transfer equation, Applied Thermal Engineering. 160 (2019) 113988. https://doi.org/10.1016/j.applthermaleng.2019.113988.
[38] S. Chaudhuri, R. Singh, K. Patwari, S. Majumdar, A. Ray, A. Singh, N. Neogi, Design and implementation of an automated secondary cooling system for the continuous casting of billets, ISA transactions. 49 (2010) 121-129. https://doi.org/10.1016/j.isatra.2009.09.005.
[39] S. Lalitha, S. Chattopadhyay, S. Das, K. Godiwalla, Simulation of heat transfer in the continuous casting mold, Transactions of the Indian Institute of Metals. 44 (1991) 89-92.
[40] J. Dantzig, Ch. Tucker, Modeling in materials processing, Cambridge university press, 2001.
[41] K. Spitzer, K. Harste, B. Weber, P. Monheim, K. Schwerdtfeger, Mathematical model for thermal tracking and on-line control in continuous casting, ISIJ international. 32 (1992) 848-856. https://doi.org/10.2355/isijinternational.32.848.